Advances in Engineering Software 40 (2009) 519–526

Contents lists available at ScienceDirect

Advances in Engineering Software

journal homepage: www.elsevier.com/locate/advengsoft

A modified boundary integral evolution formulation for the wave equation

Okey Oseloka Onyejekwe

Department of Mechanical Engineering, Northern Arizona University, Flagstaff, AZ 86011-5682, USA

ARTICLE INFO

Article history:
Received 2 July 2007
Received in revised form 18 March 2008
Accepted 21 October 2008
Available online 17 December 2008

Keywords:
Green element method
Boundary element method
Wave equation
Overhauser elements

ABSTRACT

We apply a modified boundary integral formulation otherwise known as the Green element method (GEM) to the solution of the two-dimensional scalar wave equation.

GEM essentially combines three techniques namely: (a) finite difference approximation of the time term (b) finite element discretization of the problem domain and (c) boundary integral replication of the governing equation. These unique and advantageous characteristics of GEM facilitates a direct numerical approximation of the governing equation and obviate the need for converting the governing partial differential equation to a Helmholtz-type Laplace operator equation for an easier boundary element manipulation. C_1 continuity of the computed solutions is established by using Overhauser elements. Numerical tests show a reasonably close agreement with analytical results. Though in the case of the Overhauser GEM solutions, the level of accuracy obtained does not in all cases justify the extra numerical rigor.

Published by Elsevier Ltd.

1. Introduction

With the current phenomenal success achieved by boundary based numerical techniques, there are still some issues to be resolved especially where the main operator in the governing equation is not the Laplace operator. We refer for example, to linear or non-linear non-homogeneous time dependent problems with or without source terms. The reason for this is not far fetched. Apart from the need to implement domain integration (which obviates an essential advantage of boundary integral technique), particular solutions (which are not easily found or are even non-existent for many of these problems) must be determined apriorily. Hence most boundary element based techniques often times adopt a lengthy approach before arriving at the integral formulation of the governing equation. For example the scalar wave equation is first of all converted to a Helmholtz-type equation in order to facilitate a BEM solution.

With this antecedent, it is not a surprise that the greatest issue that has dominated the BEM community for well over a decade rests on how to interpret or resolve the relationship between the problem domain and its boundary. BEM literature is now replete with methods aimed principally at the transformation of domain to boundary integrals. Foremost among these is the dual reciprocity boundary element method (DRBEM) [1] which has recorded increasing popularity due to its ease of executing fundamental solutions while keeping faith with the boundary-only specification of BEM. DRBEM has been shown to offer high accuracy in approximating spatial derivatives [2]; hence its stability as well as its overall accuracy in solving transient problems is largely influenced by the choice of time marching schemes.

Unfortunately DRBEM inherits some of the computational disadvantage of classical BEM. Their systems of algebraic equations are non-slender matrices and fully populated. Numerical difficulties also arise because of difficulties in the selection of interpolation functions for the unknown variables. The same pitfall can also be identified with the multiple reciprocity method (MRM); another boundary element technique for the conversion of domain integral to the boundary [3]. Hence despite the pioneering work relating the boundary element method to the dual reciprocity method and radial basis function [1], BEM still suffers from considerable numerical difficulties arising mostly from its handling of singular integrals, and numerical approximations originating from the transfer of domain integrals to the boundary. As a result, the transformed boundary integrals more often than not do not sufficiently replicate the original differential equation; or yield slender and sparse coefficient matrices amenable to numerical solution.

Another technique, the method of fundamental solution (MFS) [4] not only possesses spectral convergence, but high order accuracy. It has been shown to perform efficiently [5,6] when combined with DRBEM and radial basis function (RBF). Though the MFS does not require an elaborate discretization of the problem boundary, it still relies on a fictitious or artificial problem surface exterior to the problem geometry to avoid singular kernel problems.

This spate of numerical activities witnessed the emergence of yet another technique known as the boundary knot method (BKM). The BKM [7,8] is one of the more recent boundary-driven RBF techniques, aimed at approximating the inhomogeneous terms

E-mail address: okuzaks@yahoo.com

0965-9978/$ - see front matter Published by Elsevier Ltd.
doi:10.1016/j.advengsoft.2008.10.002

for any general partial differential equation. It is mesh free and is different from the MFS because it employs a non-singular general solution instead of singular fundamental solution to prevail over the artificial boundary outside of the problem domain. While methods exist for the meshless evaluation of domain integrals, it has been shown [9] that mesh-based domain integration is generally more accurate and can be performed much faster by applying the fast multipole methods or by other methods arising from the discretization of the domain into domain elements.

So far we have seen attempts concentrated on complete avoidance of the polygonalization and integral evaluations of the problem domain. Although they affirm the concepts of the boundary element method, yet their boundary nodes are coupled to each other; and as a result their associated matrices are dense, computationally less efficient to solve, and only accurate for a certain class of problems, especially those which involve very little or no interaction between the problem's boundary and its domain.

It was not until about a decade ago that a novel hybrid boundary integral methodology (GEM) [10] was introduced. GEM departs radically from previous attempts because it permits the integral replication of the governing differential equation to be evaluated within a typical element and does not consider it a disadvantage to discretizes the problem domain. Given this condition, the coefficient matrix is as sparse as that encountered in FEM, and inhomogeneity, non-linearity, heterogeneity are all handled efficiently. These merits led to tremendous improvement in the computational capacity of BEM [10–13]. Following this initial success, other variants of the GEM have started appearing in BEM literature. The multiple domain dual reciprocity method (DRM-MD) approach [14] is very similar in approach to GEM. However it still keeps faith with classical BEM by converting the domain integrals sub-domain into a series of boundary integrals by dual reciprocity with augmented thin-plate splines as interpolation functions. This approach yields smaller matrices with better condition numbers, and should provide more accurate results for certain class of problems.

Prior to these approaches cell-based techniques within the context of BEM formulations have been glossed over for different reasons. One of the primary reasons for this is that the whole concept goes against the spirit of BEM by actively engaging the problem domain in boundary integral computations. However, recent advances in BEM have cast a doubt in this belief. With the current advances made in automatic grid generation, integration techniques, it has been shown that cell-based methods are orders of magnitude faster and more accurate than meshless methods [9].

In this study, the numerical behavior of the Green element method (GEM) when it incorporates the second derivative of the time variable arising from the two-dimensional scalar wave equation as well as other non-homogeneous terms are examined. The robustness of the formulation is tested by considering the effects of viscous damping as well as the influence of distributed and point sources on the solution profiles. Effects of C_1 continuity on the accuracy of numerical results are studied by deriving a form of GEM, which uses Overhauser elements. The current presentation essentially retains the standard GEM procedure which starts with an appropriate fundamental solution and a transformation of the governing differential equation into its integral equivalent over the problem domain. Green's second identity is applied to the integral equation, but any resulting domain integral is implemented within elements (the so called Green elements) inside the problem domain. This distinguishing feature of an essentially boundary integral procedure which implements FEMs domain discretization provides a hybrid numerical technique that enhances computational accuracy and robustness.

The objective of this paper is twofold. The first is to provide further answers to continuous queries received by the author concerning the formulation and validity of GEM especially for problems hitherto unsolved by the method. The other is to illustrate how to express boundary integral equations in a simple direct form and yet applicable to challenging problems in mathematical physics and engineering. Hence we shall be restricting ourselves to a setting that aims to address these issues sufficiently so that GEM treatment of the governing equations could be appreciated.

2. Governing equation and gem formulation

2.1. GEM discretization

Some of the details provided in this section have been mentioned elsewhere [10–13], however we still provide salient aspects of GEM in order to enhance clarity. For a fairly general case, let us consider the equation governing the longitudinal vibration of a damped plate, exposed to contributions from point and distributed sources:

$$\nabla^2\phi = \frac{1}{c^2}\frac{\partial^2\phi}{\partial t^2} + \gamma\frac{\partial\phi}{\partial t} + F + Q, \tag{1}$$

where ϕ is the primary variable, $\nabla = i\partial/\partial x + j\partial/\partial y$ is the 2D gradient operator, t is time variable, γ is the velocity-dependent external viscous damping factor, c^2 is the wave speed, F and Q represent distributed and point sources, respectively. Unique solutions of Eq. (1) are obtained when appropriate initial and boundary conditions are specified on the boundary and the domain of the problems at all times. The point sources are expressed as

$$Q = \sum_{p=1}^{N_p} Q_p\delta(x - x_p)\delta(y - y_p), \tag{2}$$

where Q_p is the strength of a source located at (x_p, y_p), δ is the dirac delta function, and N_p is the number of such point sources.

The integral representation of Eq. (1) is initiated by the construction of a suitable auxiliary equation from which we obtain the free-space Green's function. After which we apply the Green's second identity to both the auxiliary equation and the governing equation to obtain a complete integral statement of the latter.

Adopting an auxiliary equation:

$\nabla^2 G = \delta(r - r_i)$ whose fundamental solution is given by $G = \ln(r - r_i)$. Eq. (1) is weighted with this fundamental solution to give

$$\int_\Omega \left(\frac{1}{c^2}\frac{\partial^2\phi}{\partial t^2} + \gamma\frac{\partial\phi}{\partial t} + F + Q - \nabla^2\phi\right) G\, d\Omega = 0. \tag{3}$$

Applying Green's second identity to (2) yields:

$$\lambda_i\phi(r_i, t) + \int_\Gamma (\phi G^* - Gq)d\Gamma + \int\int_\Omega \left(\frac{1}{c^2}\frac{\partial^2\phi}{\partial t^2} + \gamma\frac{\partial\phi}{\partial t} + F\right)d\Omega + \sum_{p=1}^{N_p} Q_p \ln(r_i - r_p) = 0, \tag{4}$$

where subscript i denotes the source point, $r = (x, y)$, $G^* = \frac{\partial G}{\partial n}$, $q = \frac{\partial\phi}{\partial n}$, Γ boundary of the domain Ω, G is the solution of the auxiliary equation. The fact that GEM involves the problem domain in dealing with Eq. (4) constitutes a major difference between GEM and other boundary-driven integral methods.

Linear shape functions are chosen to approximate the dependent variables in terms of the values at the four nodes of quadrilateral elements used for domain discretization. The resulting matrix equation is given by

$$R_{ij}\phi_j + L_{ij}q_j + T_{ij}\left(\frac{\partial^2\phi_j}{\partial t^2} + \gamma\frac{\partial\phi_j}{\partial t} + F_j\right) + \sum_{p=1}^{N_p} Q_p \ln(r_i - r_p) = 0. \tag{5}$$

Details of the coefficient matrices are treated in detail in [11], however some other key features of their evaluation are given in Appendix A. A semi-implicit finite difference approximation is adopted to approximate the time derivative at t_{m+1} as

$$\left.\frac{d^2\varphi_j}{dt^2}\right|t = t_{m+1} = \frac{d^2\varphi_{j,m+1}}{dt^2} \approx \frac{\alpha}{\Delta t^2}(\varphi_{j,m+1} - 2\varphi_{j,m} + \varphi_{j,m-1}) + (1-\alpha)\frac{d^2\varphi_{j,m}}{dt^2} \quad 1 \leqslant \alpha \leqslant 2, \tag{6}$$

where α is a time weighting factor, the subscripts $m+1$ and m represent current and previous time levels and $\Delta t = t_{m+1} - t_m$ is the time step.

To improve on the GEM results, the Overhauser elements [15] are employed to guarantee C_1 continuous solutions in a way similar to finite element method (FEM) interpolation technique. This approach, demands that more nodes be considered in the process. The dependent variable is therefore interpolated over an element by making use of both the nodal values of the element itself as well as those of the surrounding elements. For example the unknown function is approximated by constructing an interpolating polynomial that should be continuous with its derivative up to a certain order. Once the desired continuity is achieved, the solution in each domain, just like in FEM, is obtained by assembling the solution found at every element. Following a standard approach for the Overhauser elements, for the one-dimensional case, two parabolas between nodes 5,6 and 7 and 6,7 and 8 (Fig. 1) are joined respectively. This combination results in a cubic function, which is used to interpolate the dependent variable between nodes 6 and 7 in terms of the nodal values of the dependent variable at nodes, 5,6,7 and 8. The one-dimensional version of the shape functions which define the cubic are given by

$$\begin{aligned} N_5(x) &= -0.5z + z^2 - 0.5z^3, \\ N_6(x) &= 1.0 - 2.5z^2 + 1.5z^3, \\ N_7(x) &= 0.5z + 2.0z^2 - 1.5z^3, \\ N_8(x) &= -0.5z^2 + 0.5z^3, \end{aligned} \tag{7}$$

where $z \in [0,1]$. In order to obtain a two 2D equivalent of the above, appropriate one-dimensional shape functions are multiplied together. For example for a 2D element of width a and height b, the shape function of nodes 10 and 2 are given by

$$N_{10}(x,y) = N_6\left(\frac{x}{a}\right)N_7\left(\frac{y}{b}\right) = \left[1.0 - 2.5\left(\frac{x}{a}\right)^2 + 1.5\left(\frac{x}{a}\right)^3\right]\left[-0.5\left(\frac{y}{b}\right) + 2.0\left(\frac{y}{b}\right)^2 - 1.5\left(\frac{y}{b}\right)^3\right], \tag{8a}$$

$$N_2(x,y) = N_6\left(\frac{x}{a}\right)N_5\left(\frac{y}{b}\right) = \left[1.5\left(\frac{x}{a}\right)^3 - 2.5\left(\frac{x}{a}\right)^2 + 1.0\right]\left[-0.5\left(\frac{y}{b}\right) + \left(\frac{y}{b}\right)^2 - 0.5\left(\frac{y}{b}\right)^2\right]. \tag{8b}$$

Generally on any 2D element, the dependent variables are interpolated as

$$\phi(x,y) = \sum_{j=1}^{16} N_j(x,y)\phi_j, \tag{9a}$$

$$q_j(x,y) = \sum_{j=1}^{16} \frac{\partial N_j}{\partial n}\phi_j. \tag{9b}$$

Nodes may not be available to carry out summation for elements situated on the boundary of the computational domain. In this case we have to fit a cubic through other known values of the dependent variable. For example the nodal value of the dependent variable at node 12 is given by

$$\phi_8 = 3\phi_7 - 3\phi_6 + \phi_5. \tag{10}$$

It is pertinent to comment that the Overhauser elements unlike the Hermitian elements carry out interpolation over the elements in terms of the unknown scalar variable only, and do not get involved with the spatial derivatives. Hence for the GEM formulation, no extra equations are needed except that more element integrals are used to account for the extra communication between nodal values as required in the summation (Eq. (9)). The required integrals are shown in Appendix B.

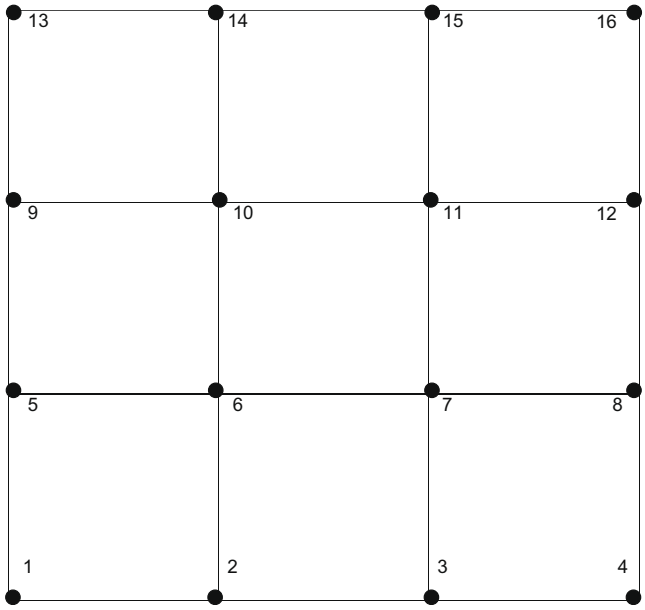

Fig. 1. A typical grid for Overhauser element.

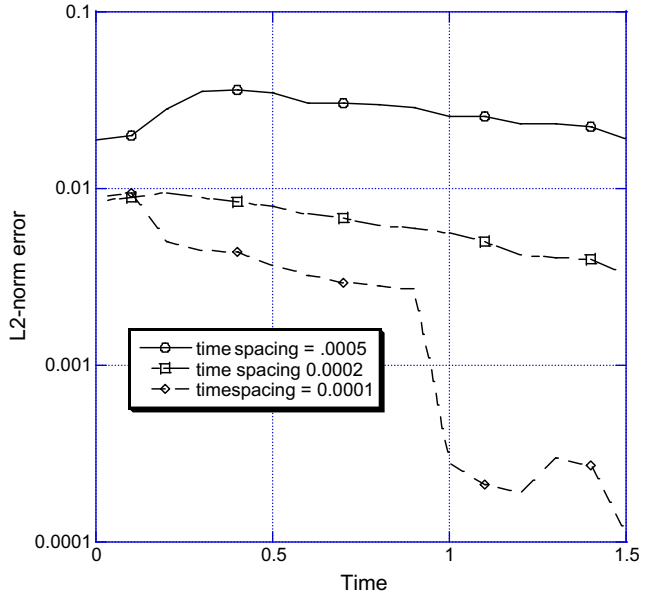

Fig. 2. L_2 norm error plots for different time intervals (grid size 11×6).

3. Numerical experiments

Example 1. We validate GEM formulation for the work reported herein by comparing GEM solutions with a closed form solution of Eq. (1) for the case of vibration of a rectangular membrane. The problem domain is assigned the following dimensionless parameters: width (along x-axis) = 4.0, length (along y-axis) = 2.0, acoustic speed $= \sqrt{25}$, initial velocity = 0.0, external viscous damping factor $\lambda = 0.0$, distributed and concentrated sources $F = Q = 0.0$, initial displacement is $\phi(x,y) = 0.1(4x - x^2)(2y - y^2)$.

Using Fourier series, the closed form solution is given by

$$\phi(x,y,t) = 0.426050 \times \left(\begin{array}{l} \cos\frac{5\pi\sqrt{5}}{4}t \sin\frac{\pi x}{4}\sin\frac{\pi y}{2} + \frac{1}{27}\cos\frac{5\pi\sqrt{37}}{4}t\sin\frac{\pi x}{4}\sin\frac{3\pi y}{2} + \\ \frac{1}{27}\cos\frac{5\pi\sqrt{13}}{4}t\sin\frac{3\pi x}{4}\sin\frac{\pi y}{2} + \frac{1}{729}\cos\frac{5\pi\sqrt{45}}{4}t\sin\frac{3\pi x}{4}\sin\frac{3\pi y}{2} + \\ \ldots\ldots\ldots\ldots \end{array} \right).$$

The overall accuracy of GEM solutions with and without the Overhauser elements is determined by L_2 norm errors defined by $\|\varphi\|_2 = \left(\frac{1}{N+1}\sum_{i=1}^{N}(\varphi_{num} - \varphi_{exact})_i^2\right)^{\frac{1}{2}}$, where N is the number of nodes, ϕ_{num},ϕ_{exact} are numerical and closed form solutions, respectively. The simulation was carried out with the following time steps: $\Delta t = 0.0005$, 0.0002, 0.0001 and 11×6 grid size. Fig. 2 shows that the L_2 norm errors decreases as the time step is decreased; with the least errors recorded for $\Delta t = 0.0001$. No significant error decrease was obtained for any further reduction in time step. Next, the time steps were kept the same, while the grid size was increased to 22×12 to test the effect of grid size on L_2 errors. There were no dramatic error changes in all the three simulations (Fig. 3). The least error change was noticed for $\Delta t = 0.0001$. Therefore, an optimum grid size-time step combination of 11×6, a time step size of $\Delta t = 0.0001$, together with an initial scalar displacement (Fig. 4) were applied for subsequent computations where the closed form solutions are not available.

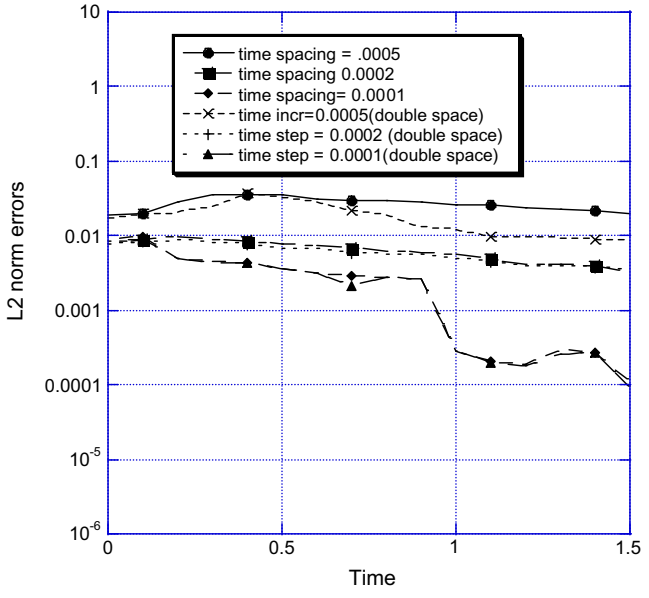

Fig. 3. L_2 norm error plots for different time intervals (grid size 22×12).

Example 2. GEM guarantees that contributions for concentrated sources or sinks are accurately reflected in the element where the node is located. It is this feature that makes GEM computationally attractive in handling singularities arising from oil well drilling, water extraction from an aquifer or concentrated pressure sources or sinks in acoustics. In order to assess the effects of specifying a concentrated source, we set $\gamma = 0.0$ and $F = 0.0$ in Eq. (1), while specifying the positions and strengths of concentrated loads on the problem domain (Table 1). This scenario is simulated with 11×6 grids with the optimum time step used for the previous example. The ability of GEM to accurately reflect both the strengths and positions of the source terms is accurately represented by Fig. 5. The figure shows local singularities as represented by the dependent variables in the locality where the sources are in accord with the problem specification.

Example 3. The next thing we want to verify is the influence of the velocity-dependent viscous damping factor on the solution profile. To that extent, we set $F = Q_p = 0.0$, and allow the second term on the right hand side of Eq. (1) to feature in the simulation, by specifying values for γ. Figs. 6 and 7 show the plots for $\gamma = 400.0$, 1000.0, respectively. The effects of viscous damping on the solution profile are clearly illustrated. The negative sign before the damping component in Eq. (1) serves to indicate that the damping force is

Table 1

Element	x-Coordinate	y-Coordinate	Q_p
26	2.5	1.0	100.0×10^3
39	3.3	1.4	100.0×10^3
12	0.63	0.47	150.0×10^3

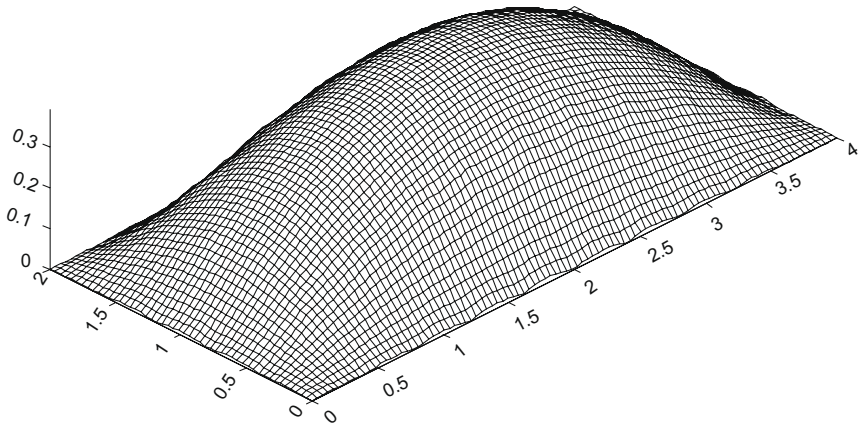

Fig. 4. Profile of initial displacement at time = 0.

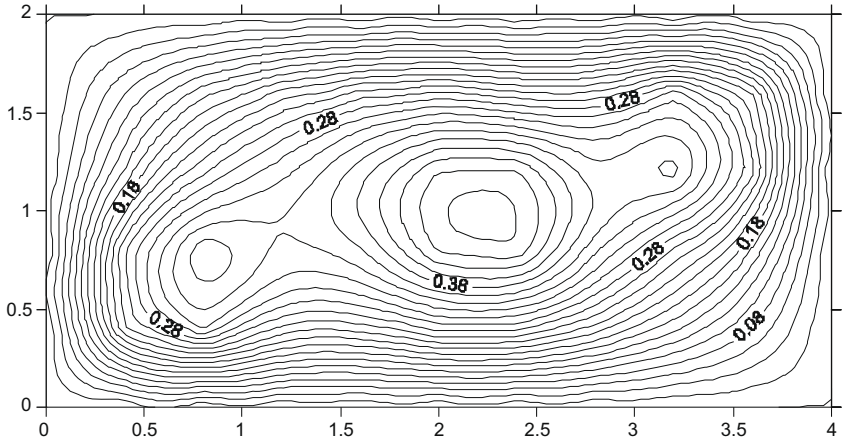

Fig. 5. Effect of source term on solution profile.

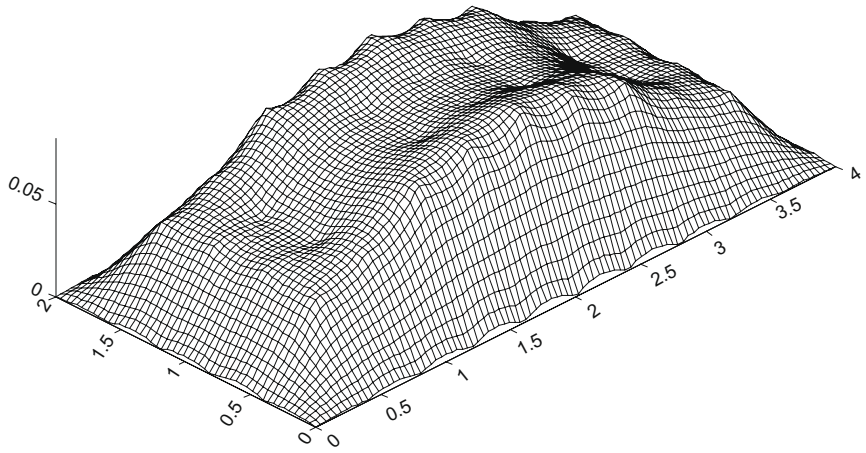

Fig. 6. Effect of viscous damping on solution profile ($\gamma = 400$).

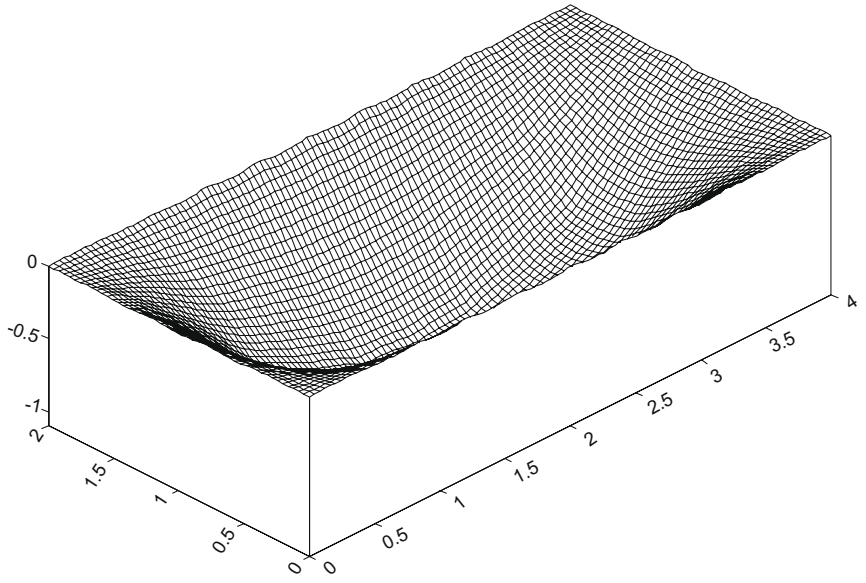

Fig. 7. Effect of viscous damping on solution profile ($\gamma = 1000$).

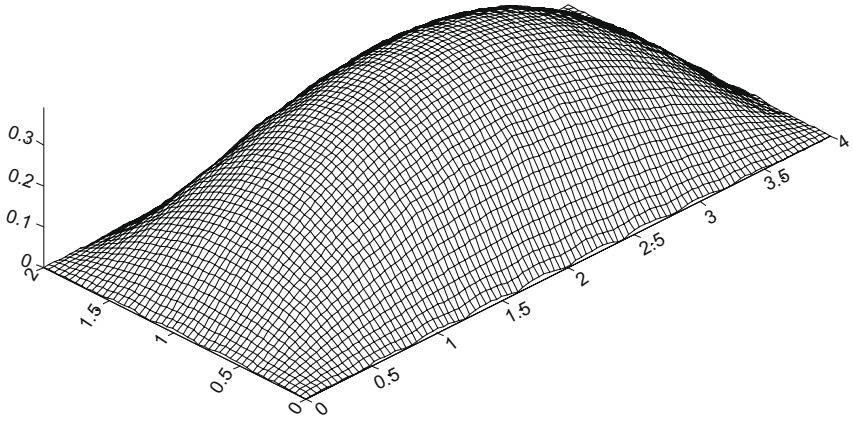

Fig. 8. Effect of distributed source on solution profile ($F = 10^3$).

opposite the direction of motion as the vibrating system is dissipated as friction or heat or transmitted by sound. Fig. 7 shows a system that is diminished in magnitude especially in the vicinity of the regions formerly displaying the highest amplitude. The total effect on the scalar profile becomes dramatic when γ assumes a much higher value. Fig. 7 shows a flip over of almost 180° when $\gamma = 1000.0$ as the damping force opposes the motion of the vibrating system. On the other hand, when a distributed source or 'recharge' is introduced into the system, say specify $F = 3.0 \times 10^3$, it can be seen that the net effect becomes immediately noticeable as the shape of the scalar profile comes very close to that of the initial condition (Fig. 8).

4. Conclusions

As most researchers in this field of study know, there are now two distinct ways of tackling boundary integral problems: an approach that strives to keep faith with classical boundary element concept of avoiding the problem domain either initially or eventually or another approach that is fast gaining credence namely adopting a finite element-like domain discretization [9–14,16,17]. Needless to say, each approach has both theoretical and pedagogical merit. While each has its own pitfall as well, it is now evident that the boundary element method (BEM) has basically two different approaches for solving problems and whichever method that is finally adopted depends on the problem at hand and the complexity of the physics it seeks to address.

Appendix A. Evaluation of element integrals

In order to solve the matrix equation in the text, we need to evaluate element integrals:

$$R_{ij} = \int_{\Gamma^e} \frac{\partial G(r, r_i)}{\partial n} N_j \, d\Gamma - \delta_{ij}\theta_i, \quad L_{ij} = -\int_{\Gamma^e} G(r, r_i) N_j \, d\Gamma,$$

$$T_{ij} = \int \int_{\Omega^e} G(r, r_j) \, d\Omega.$$

Details of this process have already been reported by Mamoli [9] where they are evaluated analytically. For a rectangular element with sides a and b, the coefficients are given as

$$R_{11} = -\frac{\pi}{2}, \tag{A.1}$$

$$R_{12} = -\frac{a}{2b} \ln\left(\frac{a^2+b^2}{a^2}\right) + \tan^{-1}\left(\frac{b}{a}\right), \tag{A.2}$$

$$R_{13} = \frac{a}{2b} \ln\left(\frac{a^2+b^2}{a^2}\right) + \frac{b}{2a} \ln\left(\frac{a^2+b^2}{a^2}\right), \tag{A.3}$$

$$R_{14} = -\frac{b}{2a} \ln\left(\frac{a^2+b^2}{b^2}\right) + \tan^{-1}\left(\frac{a}{b}\right). \tag{A.4}$$

The remaining elements in the R_{ij} matrix are expressed by the following relationships:

$$R_{ii} = R_{11}, \tag{A.5}$$

$$R_{ij} = R_{ji}, \tag{A.6}$$

$$R_{23} = R_{14}, \tag{A.7}$$

$$R_{24} = R_{13}, \tag{A.8}$$

$$R_{34} = R_{12}. \tag{A.9}$$

The flux is split into two to account for flux before and after a node when integrating in a counter clockwise direction. Here we give analytic expressions for the flux. In all cases the superscripts b and a denote flux before and after a generic node, respectively.

$$L_{11}^b = -b\frac{\left(\ln b^2 - 3\right)}{4}, \tag{A.10}$$

$$L_{12}^b = -a\frac{\left(\ln a^2 - 1\right)}{4}, \tag{A.11}$$

$$L_{11}^f = -a\frac{\left(\ln a^2 - 3\right)}{4}, \tag{A.12}$$

$$L_{12}^f = -\frac{1}{4}\left[b\ln(a^2+b^2) - \frac{a^2}{b}\ln\frac{(a^2+b^2)}{a^2} - 3b + 4a\tan^{-1}\frac{b}{a}\right], \tag{A.13}$$

$$L_{13}^b = -\frac{1}{4}\left[b\ln(a^2+b^2) + \frac{a^2}{b}\ln\frac{(a^2+b^2)}{a^2} - b\right], \tag{A.14}$$

$$L_{13}^f = -\frac{1}{4}\left[a\ln(a^2+b^2) + \frac{b^2}{a}\ln\frac{(a^2+b^2)}{b^2} - a\right], \tag{A.15}$$

$$L_{14}^b = -\frac{1}{4}\left[a\ln(a^2+b^2) - \frac{b^2}{a}\ln\frac{(a^2+b^2)}{b^2} - 3a + 4b\tan^{-1}\frac{a}{b}\right], \tag{A.16}$$

$$L_{14}^f = -b\frac{(\ln b^2 - 1.0)}{4.0}. \tag{A.17}$$

Eqs. (A.10)–(A.17) serve as a basis for linking the remaining terms of the 4×4 matrices that describe L^f_{ij} and L^b_{ij}. They occur in this fashion

$$\begin{aligned}
&L^f_{12} = L^b_{21}, \quad L^f_{11} = L^b_{22}, \quad L^f_{14} = L^b_{23}, \quad L^f_{13} = L^b_{23}, \quad L^f_{12} = L^f_{34},\\
&L^f_{21} = L^b_{12}, \quad L^f_{22} = L^b_{11}, \quad L^f_{23} = L^b_{14}, \quad L^f_{24} = L^b_{13}, \quad L^f_{31} = L^f_{13},\\
&L^f_{32} = L^f_{14}, \quad L^f_{33} = L^f_{11}, \quad L^f_{34} = L^f_{12}, \quad L^f_{41} = L^f_{14}, \quad L^f_{42} = L^b_{13},\\
&L^f_{43} = L^b_{12}, \quad L^f_{44} = L^b_{11}, \quad L^f_{33} = L^b_{11}, \quad L^f_{34} = L^b_{12}, \quad L^f_{34} = L^b_{12},\\
&L^f_{41} = L^f_{14}, \quad L^f_{42} = L^f_{13} \quad L^f_{43} = L^f_{12}, \quad L^f_{44} = L^f_{11}, \quad L^b_{31} = L^b_{13},\\
&L^b_{32} = L^b_{14}.
\end{aligned}$$

Problems involving time derivative, as well as source and sink terms require that the coefficient T_{ij} be evaluated. In order to avoid the tedium involved in computing the matrix elements analytically, we have elected to adopt a numeric-symbolic integration of the component terms to yield:

$$T_{11} = \frac{1}{ab}\begin{pmatrix} -0.520833a^2b^2 + 0.16667\left(ab^3 \arctan\left(\frac{a}{b}\right) + a^3 b \arctan\left(\frac{b}{a}\right)\right) + 0.02083333 \\ (a^4\log(a^2) + b^4\log(b^2) - a^4\log(a^2+b^2) - b^4\log(a^2+b^2)) + 0.125a^2b^2\log(a^2+b^2) \end{pmatrix}, \tag{A.18}$$

$$T_{12} = \frac{1}{ab}\begin{bmatrix} -0.395833a^2b^2 + 0.3333a^3 b \arctan(\frac{b}{a}) \\ +0.0625a^4(\log(a^2) - \log(a^2+b^2)) \\ +0.125a^2b^2\log(a^2+b^2) + 0.0625a^4(\log(a^2) - \log(a^2+b^2)) \\ +0.0208333(b^4\log(a^2+b^2) - b^4\log(b^2)) \end{bmatrix}, \tag{A.19}$$

$$T_{13} = \frac{1}{ab}\begin{bmatrix} -0.1875a^2b^2 + 0.0625\begin{pmatrix}(a^4+b^4)\log(a^2+b^2) - a^4\log(a^2) \\ -b^4\log(b^2)\end{pmatrix} \\ +0.125a^2b^2\log(a^2+b^2) \end{bmatrix}, \tag{A.20}$$

$$T_{14} = \frac{1}{ab}\begin{bmatrix} -0.395833a^2b^2 + 0.33333ab^3 \arctan\left(\frac{a}{b}\right) \\ +0.02083333a^4(\log(a^2+b^2) - \log(a^2)) \\ +0.0625b^4(\log(b^2) - \log(a^2+b^2)) \\ +0.125a^2b^2\log(a^2+b^2) \end{bmatrix}. \tag{A.21}$$

The remaining terms are defined by symmetry, and are given as

$$T_{ij} = T_{ji}, \quad T_{ii} = T_{11}, \quad T_{12} = T_{34}, \quad T_{13} = T_{24}, \quad T_{14} = T_{23}.$$

Appendix B. Matrix for Overhauser elements

The Overhauser elements are introduced to guarantee C_1 continuity of the primary dependent variable. This requires that the coefficient matrix for the primary dependent variable be recomputed to reflect the fact that 16 positions are now required for the field node of the Green function. While the definition of the R_{ij} matrix remains the same;

$$R_{ij} = \int_{\Gamma^e} \frac{\partial G(r, r_i)}{\partial n} N_j d\Gamma - \delta_{ij}\theta_i \tag{B.1}$$

the shape functions N_j are no longer linear. The new values of the R_{ij} matrix are given as

$$R_{11} = -\frac{\pi}{2}, \tag{B.2}$$

$$R_{12} = \frac{1}{b^3}\begin{bmatrix} -1.75a^2b + (2.5a^2b + b^3)\arctan(\frac{b}{a}) \\ +0.75a^3\log(a^2) - 0.75a^3\log(a^2+b^2) \end{bmatrix}, \tag{B.3}$$

$$R_{13} = -\frac{b}{a^3}\begin{bmatrix} -1.25a^2 + 2ab\arctan\left(\frac{b}{a}\right) + (0.25a^2 + 0.75b^2)\log(b^2) \\ -0.25a^2\log(a^2+b^2) - 0.75b^2\log(a^2+b^2) \\ +\frac{a}{b^3}(1.25b^2) - 2ab\arctan\left(\frac{b}{a}\right) + (-0.75a^2 - 0.25b^2)\log(a^2) \\ +0.75a^2\log(a^2+b^2) + 0.25b^2\log(a^2+b^2) \end{bmatrix}, \tag{B.4}$$

$$R_{14} = -\frac{1}{a^3}\begin{bmatrix} 1.75a^2b + (-a^3 - 2.5ab^2)\arctan\left(\frac{a}{b}\right) \\ +0.75b^3\log(b^2) + 0.75b^3\log(a^2+b^2) \end{bmatrix}, \tag{B.5}$$

$$R_{16} = \frac{a}{b^3}\begin{bmatrix} 0.75b^2 - ab\arctan\left(\frac{b}{a}\right) + 0.25(b^2 - a^2)\log(a^2) \\ +0.25a^2\log(a^2+b^2) - 0.25b^2\log(a^2+b^2) \end{bmatrix}, \tag{B.6}$$

$$R_{17} = \frac{a}{b^3}\begin{bmatrix} 0.75a^2 - ab\arctan\left(\frac{a}{b}\right) + 0.25(b^2 - a^2)\log(b^2) \\ +0.25a^2\log(a^2+b^2) - 0.25b^2\log(a^2+b^2) \end{bmatrix}, \tag{B.7}$$

$$R_{1,10} = -\frac{b}{a^3}\begin{bmatrix} -0.5ab\arctan\left(\frac{a}{b}\right) - 0.25b^2\log(b^2) \\ +0.25(a^2 + b^2\log(a^2+b^2)) \end{bmatrix}, \tag{B.8}$$

$$R_{12} = \frac{a}{b^3}\left[0.5\arctan\left(\frac{b}{a}\right) + 0.25a^2\log(a^2) - 0.25\left(b^2 + a^2\log(a^2+b^2)\right)\right], \tag{B.9}$$

The following elements are related by symmetry:

$$R_{11} = R_{ii} \quad i = 2,3,4 \qquad R_{ij} = R_{ji}, \quad i,j = 2,3,4,$$

$$R_{16} = R_{4,12} = R_{47} = R_{38} = R_{3,11} = R_{2,10} = R_{25},$$

$$R_{1,10} = R_{29} = R_{2,11} = R_{35} = R_{37} = R_{48} = R_{46}$$

all zero terms are unspecified.

References

[1] Nardini D, Brebbia CA. A new approach to free vibration analysis using boundary elements. Appl Math Model 1983;7:157–62.

[2] Chen CS, Brebbia CA, Power H. Dual reciprocity method using compactly supported radial basis functions. Commun Numer Methods Eng 1999;15:137–50.

[3] Chen JT, Wong WC. Dual formulation of multiple reciprocity method for the acoustic mode of a cavity with a thin partition. J Sound Vibrat 1998;47:75–95.

[4] Bogonolny A. Fundamental solutions method for elliptic boundary value problems. SIAM J Numer Anal 1985;22:644–69.

[5] Chen CS, Marcozzi M, Choi S. The method of fundamental solutions and compactly supported radial basis functions – a meshless approach in 3D

problems. In: Brebbia CA, Power H, editors. Boundary element methods, XXI. WIT Press; 1999. p. 561–70.
[6] Fairweather G, Karageorghis A. The method of fundamental solution for elliptic boundary problems. Adv Comput Math 1998;9:69–95.
[7] Hon YC, Chen W. Boundary knot method for 2D and 3D Helmholtz and convection–diffusion problems with complicated geometry. Int J Numer Methods Eng 2003;56:1931–48.
[8] Chen W, Hon YC. Numerical convergence of boundary knot method in the analysis of Helmholtz modified, Helmholtz and convection–diffusion problems. Comput Methods Appl Mech Eng 2003;192:1859–75.
[9] Mamoli AA. Solution of nonlinear boundary integral equations in complex geometries with auxiliary integral subtractions. Int J Numer Methods Eng 2002;55:1115.
[10] Taigbenu AE. The Green element method. Int J Numer Methods Eng 1995;38:2241–63.
[11] Taigbenu AE. The Green element method. Boston: Kluwer Academic Publishers; 1999. 377p.
[12] Onyejekwe OO. Green element method for 2D Helmholtz and convection diffusion problems with variable velocity coefficients. Numer Methods Part Differ Equat 2005;21:229–41.
[13] Onyejekwe OO. An efficient Green element algorithm for radial flow. Appl Math Comput 2005;165:635–45.
[14] Popov V, Power H. The DRM-MD integral equation method: an efficient approach for the numerical solution of domain dominant problems. Int J Numer Methods Eng 1999;44:327.
[15] Hall WS, Hibbs TT. Continuous quadrilateral and triangular surface patches. In: Creasy CFM, Craggs C, (editors). Applied surface modeling, 1990. p. 139.
[16] Archer RA, Horne RN. Green element method and singularity programming for numerical well test analysis. Eng Anal Bound Elem 2002;29:537–46.
[17] Archer RA, Horne RN, Onyejekwe OO. Petroleum reservoir applications of the dual reciprocity boundary element method and the Green element method. In: Proceedings 21st world conference on the boundary element method, August 25–27, Oxford University; 1999.